HEFAT2012
9th International Conference on Heat Transfer, Fluid Mechanics and Thermodynamics
16 – 18 July 2012
Malta

RAYLEIGH-BÉNARD CONVECTION IN A CYLINDER WITH AN ASPECT RATIO OF 8

Leong S.S.
School of Mechanical and Manufacturing Engineering,
The University of New South Wales,
Sydney, 2052,
Australia,
E-mail: s.leong@unsw.edu.au

ABSTRACT

The three-dimensional time-dependent Navier-Stokes equations (Boussinesq approximation) for an incompressible viscous fluid are approximated using finite-differences. A uniform cylindrical mesh consisting of *L*x*M*x*N* discrete points in the radial (r), azimuthal (ϕ) and axial (z) directions respectively is superimposed on the solution domain. The energy and vorticity transport equations are solved using a modified transient Samarskii-Andreyev ADI scheme. The elliptic equation for the vector-potential is solved using by direct Fourier series using a fast Fourier transform algorithm. Transient numerical solutions of time dependent three-dimensional equations for Rayleigh-Bénard convection in a vertical cylinder are presented. Results are presented for aspect ratio (radius to height) of 8, a Prandtl number Pr=7 and Rayleigh numbers $1000 \le Ra \le 20000$.

INTRODUCTION

Fluid motion driven by convection (due to thermal gradients) is a common and important phenomenon in nature. It is important in storage of fluids, solar collectors, crystal growth and industrial processes. Natural convection in a shallow horizontal fluid layer has been extensively studied in rectangular containers with the upper and lower surfaces cooled and heated respectively and the vertical walls insulated [1-3]. Rectangular container with conducting vertical walls was studied experimentally by Stock and Müller [4] and theoretically by Davis [5]. A closed vertical cylinder was used by Müller *et al*. [6] for their experimental and theoretical studies for aspect ratios between 0.1 and 1.0. The three-dimensional numerical results of Leong [7] for aspect ratios of 2 and 4 showed that the heat transfer is dependent on the flow structure. Liu and Ahlers [8] used aspect ratio of 30 in their experimental study of Rayleigh-Bénard convection in pure gases and binary gas mixtures. . Cioni *et al*. [9] used aspect ratio of 0.5 in their experimental study in mercury and water at high-Rayleigh numbers.

In the present numerical study, the top surface of a vertical cylindrical container is cooled, the bottom surface is heated, the vertical cylindrical wall is adiabatic and the initial interior temperature is the average of the top and bottom temperature. The vertical temperature gradient creates a buoyancy-driven flow within the cylinder. Depending on the Rayleigh number *Ra*, heat is initially transferred by conduction only and there is no motion. Convection only starts when *Ra* exceeds a critical Rayleigh number Ra_c. The resulting natural convection can be simple or complex three-dimensional flow structures. It is also possible to have more than one flow structure for a given *Ra*.

NOMENCLATURE

a	aspect ratio, R/H
H	height of cylinder
KE	relative kinetic energy
L	number of radial mesh points
M	number of azimuthal mesh points
N	number of axial mesh points
Nu	Nusselt number
Pr	Prandtl number
R	radius of cylinder
Ra	Rayleigh number
r	radial coordinate
t	dimensionless time
$\overline{U}$	velocity vector
u	radial velocity
v	azimuthal velocity
w	axial velocity
z	axial coordinate
ϕ	azimuthal coordinate
θ	dimensionless temperature
υ	kinematic viscosity
κ	thermal diffusivity

$\overline{\psi}$ vector potential

$\overline{\zeta}$ vorticity vector

Subscripts

h hot

c cold

ϕ azimuthal component

r radial component

z axial component

GOVERNING EQUATIONS

The energy and momentum equations are non-dimensionalised using H (height of the cylinder), H^2/κ and κ/H as scale factors for length, time and velocity respectively. κ is the fluid thermal diffusivity. Applying the Boussinesq approximation, the energy and vorticity transport equations are given by:

$$\frac{\partial \theta}{\partial t} = -\nabla \bullet (\overline{U}\theta) + \nabla^2 \theta \qquad (1)$$

$$\frac{\partial \overline{\zeta}}{\partial t} = -\nabla \times (\overline{U} \times \overline{\zeta}) - RaPr\nabla \times (\theta \overline{g}) - Pr\nabla \times (\nabla \times \overline{\zeta}) \qquad (2)$$

where $\theta=(T-T_o)/\Delta T$ is the dimensionless temperature, $T_o=(T_h+T_c)/2$, $\Delta T=(T_h-T_c)$ and T_h and T_c are the temperature at the hot lower and cold upper surfaces respectively. $\overline{\zeta}$ is the vorticity vector, $Pr=\upsilon/\kappa$ is the Prandtl number, $Ra=\beta g(T_h-T_c)R^3/\upsilon\kappa$ is the Rayleigh number and υ is the kinematic viscosity. The components of the velocity vector $\overline{U}$ are u, v and w in the radial (r), azimuthal (ϕ and axial (z) directions respectively. The velocity is obtained from a solenoidal vector potential field $\overline{\psi}$, which satisfies the continuity equation and the curl of which gives the velocity field, that is:

$$\nabla \bullet \overline{\psi} = 0 \qquad (3)$$

$$\overline{U} = \nabla \times \overline{\psi} \qquad (4)$$

The relationship between vorticity $\overline{\zeta}$ and vector potential $\overline{\psi}$ is given by:

$$\overline{\zeta} = \nabla \times \overline{U} = \nabla \times \left(\nabla \times \overline{\psi} \right) \qquad (5)$$

BOUNDARY CONDITIONS

The fluid has zero velocities at the rigid walls ($u=v=w=0$). The thermal boundary conditions are $\theta=0.5$ and $\theta=-0.5$ at the heated bottom and cooled top isothermal horizontal surfaces respectively and adiabatic at the vertical curved cylindrical wall. The vorticity boundary conditions, in terms of the vector potential, are:

at $z=0,1$

$$\zeta_r = -\frac{\partial^2 \psi_r}{\partial z^2}; \quad \zeta_\phi = -\frac{\partial^2 \psi_\phi}{\partial z^2}; \quad \zeta_z = 0$$

at $r=a$

$$\zeta_r = 0; \quad \zeta_z = -\frac{\partial}{\partial r}\left(r\frac{\partial \psi_z}{\partial r}\right) \quad \text{and}$$

$$\zeta_\phi = -\frac{\partial}{\partial r}\left(r\frac{\partial \psi_\phi}{\partial r}\right) - 2\frac{\partial \psi_r}{\partial \phi}$$

The boundary conditions for the vector potential are:

$$\frac{\partial r\psi_r}{\partial r} = \psi_z = \psi_\phi = 0 \qquad \text{at } r=a$$

$$\frac{\partial \psi_z}{\partial z} = \psi_r = \psi_\phi = 0 \qquad \text{at } z=0,1$$

NUMERICAL SOLUTION

A uniform mesh consisting of $LxMxN$ discrete points in the r-, ϕ- and z- directions respectively is superimposed on the solution domain so that the radial mesh points are given by $r_i=(i-\frac{1}{2})\Delta r$ for $i=1,2,3,...L$; the azimuthal mesh points are given by $\phi_j=(j-1)\Delta\phi$ for $j=1,2,3,...M$ and the axial mesh points are given by $z_k=(k-1)\Delta z$ for $k=1,2,3,...N$, where $\Delta r=a/(L-\frac{1}{2})$, $\Delta\phi=2\pi/M$ and $\Delta z=1/(N-1)$. This mesh avoids the singularity at the axis. Using this mesh, centred finite difference approximations are used for equations (1) and (2), except at $r=\Delta r/2$ (i.e. $i=1$) where second order forward differences are used for the radial derivatives. The resulting finite difference equations are then solved using a modified Samarskii-Andreyev alternating direction implicit (ADI) scheme (Samarskii and Andreyev [10]. The elliptic equation (5) is solved by direct Fourier series (Le Bail [11]) using the fast Fourier transform algorithm of Cooley and Tukey [12]. Details of the solution procedure are reported by Leong [13].

Initial Conditions

The initial velocities, vorticities and vector-potentials in the solution domain and at the rigid walls were all set to zeros. The thermal boundary conditions are $\theta = 0.5$ and $\theta = -0.5$ at the heated lower and cooled upper isothermal horizontal surfaces respectively. The temperatures at all the interior mesh-points and at the vertical cylindrical wall are set to $\theta = 0$.

RESULTS

Solutions are obtained for Prandtl number $Pr=7$ and various Rayleigh number (Ra) using an aspect ratio of 8. For Rayleigh numbers $Ra \leq 1860$, the fluid is thermally stratified, there is no convection and heat is transferred only by conduction. The Nusselt number Nu, representing heat transfer from the heated lower surface to the fluid in the cylinder is evaluated using

$$Nu = -\int_0^{2\pi}\int_0^{a} r\frac{d\theta}{dz}drd\phi$$

is equal to 201.1 which is the same value for pure conduction. A relative kinetic energy evaluated using

$$KE = \frac{1}{\pi a^2}\iiint \tfrac{1}{2}V^2 rd\phi drdz$$

is used to give the strength of the flow within the cylinder. For $Ra \le 1860$ there is no motion and *KE* is equal zero.

When *Ra*=1880, convection is very weak and at steady state *Nu*=201.3. The Nusselt number of 201.2 will be used to indicate when pure conduction ends and convection starts. The duration of the pure conduction phase is 265.2. The value of *KE* at steady state is 0.02842. Figure 1 shows the transient plot of *Nu* for *Ra*=1900. The initial sharp drop in *Nu* is due to the interior temperature being set at zero and therefore the initial high temperature gradient at both the upper and lower ends of the cylinder. There is no fluid motion and heat is transferred by pure conduction. This pure conduction phase ends at t=63.21 when *Nu*=201.2 and convection starts. At steady state *Nu*=202.4. Figure 2 shows the transient plot of *KE* for *Ra*=1900. Initially there is no motion during the pure conduction phase. As convection starts, *KE* increases in value and at steady state it is equal to 0.1474.

Figure 3 shows the isotherms and aximuthal component ψ_ϕ of the vector-potential in a vertical plane for *Ra*=1900 at steady state. The contour plots show the range of the contour values and the number of levels. There are 15 rolls and the strength of the rolls decreases away from the axis of the cylinder. The central roll rotates about the diameter and all the other rolls rotate about semi-circular arcs. Figure 4(a) shows the isotherms at the horizontal mid-height plane (*z*=0.5). Figures 4(b) and 4(c) show axial velocity (*w*) contours and profile respectively at the horizontal mid-height plane (*z*=0.5). The isotherms and *w* contours two contours plots look very similar and therefore only temperature contours will be used to display the flow structure of higher Rayleigh numbers.

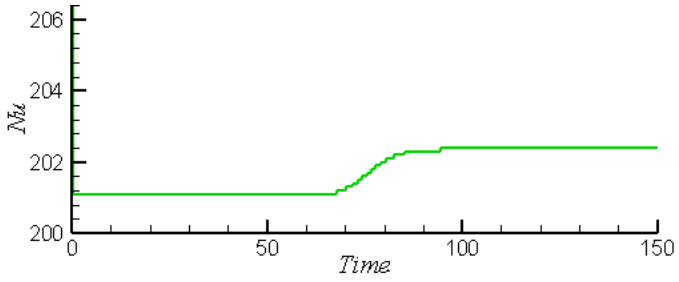

Figure 1 Transient plot of *Nu* for *Ra*=1900.

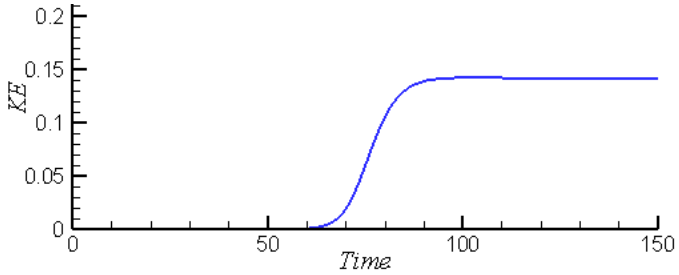

Figure 2 Transient plot of *KE* for *Ra*=1900.

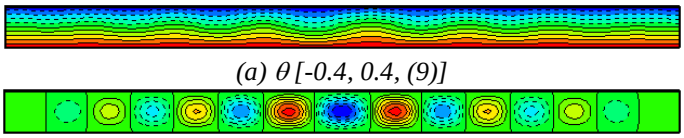

(a) θ [-0.4, 0.4, (9)]

(b) ψ_ϕ [-0.6, 0.6, (13)]

Figure 3 Contour plots of ψ_ϕ and θ respectively in the vertical plane for *Ra*=1900.

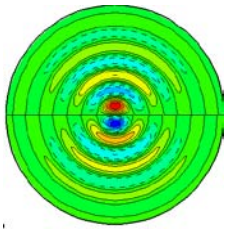

(a) θ [-0.1, 0.1, (11)]

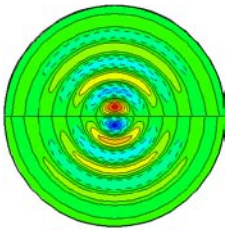

(b) w [-2.4, 2.4, (11)]

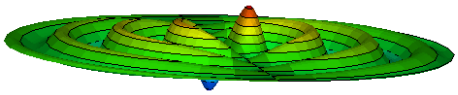

(c) w [-2.4, 2.4, (11)]

Figure 4 Isotherms and contour plots and profile of axial velocity (*w*) at horizontal mid-height plane (z=0.5) at steady state for *Ra*=1900

Figure 5 and 6 show transient plots of *Nu* and *KE* respectively for *Ra*=2000. The pure conduction phase is now much shorter and convection starts at t=8.47. *Nu* increases sharply to 228.3 where it remains constant for a while before increasing to 229.1 at steady state. *KE* increases to 3.50 after convection has started an remains constant during this convection phase before changing to 3.605 at steady state.. Figure 7 shows the isotherms and ψ_ϕ in the vertical plane at t=305. Figure 8 shows isotherms at mid-height plane (z=0.5) at various times. At t=15, the isotherms are semi-circular in shape. This is the convection phase after the pure conduction phase, It then starts to merge at t=36 to form spirals. These spirals rotate very slowly in a clockwise direction about the axis of the cylinder. During this rotation, *Nu* and *KE* remain constant.

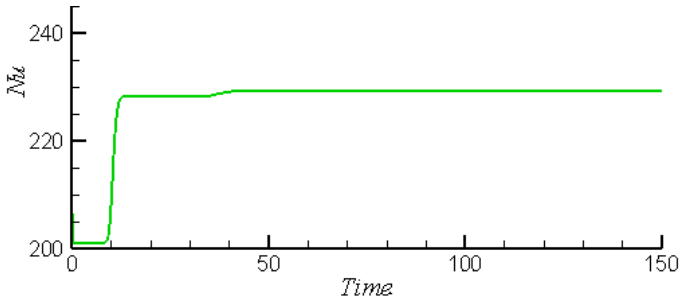

Figure 5 Transient plot of *Nu* for *Ra*=2000.

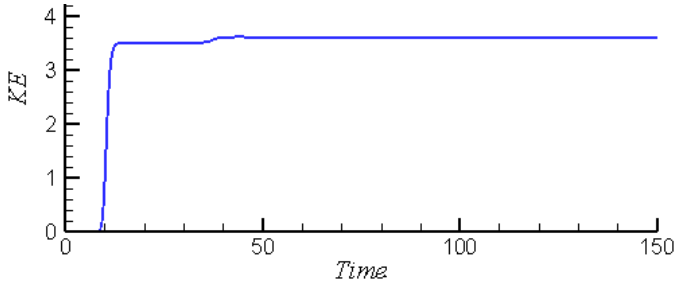

Figure 6 Transient plot of *KE* for *Ra*=2000.

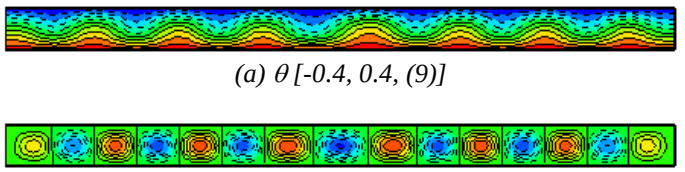

(a) θ [-0.4, 0.4, (9)]

(b) ψ_ϕ [-1.5, 1.5, (13)]

Figure 7 Contour plots of ψ_ϕ and θ respectively in the vertical plane for *Ra*=2000.

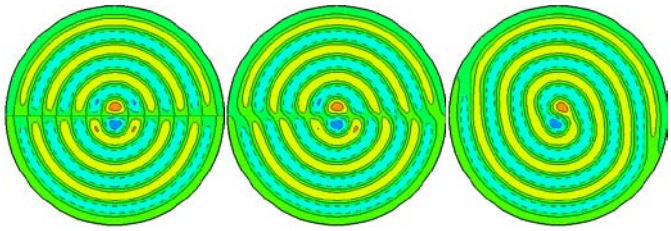

(a) t=15 (b) t=36.8 (c) t=305

θ [-0.2, 0.2, (5)]

Figure 8 Isotherms at horizontal mid-height plane (z=0.5) at various times for *Ra*=2000.

Figure 9 and 10 show transient plots of NU and *KE* for *Ra*=4000. The pure conduction phase ends at t=1.17 when convection starts. At t=2.8, semi-circular rolls are formed as shown in Figure 11. At this time there are 17 rolls in the vertical plane. These semi-circular rolls then start to merge to form spirals (t=6.2, 12.6 and 15.0). At t=15.0, the completed spirals start to rotate in a clockwise direction. The number of rolls in the vertical plane is now reduced to 13. At t=70.6, it has rotated through almost 90º and at t=123.9 it has rotated through a complete cycle. The period of this rotation is 106.5. The values of *Nu* and *KE* during the steady rotation are 374.6 and 43.88 respectively.

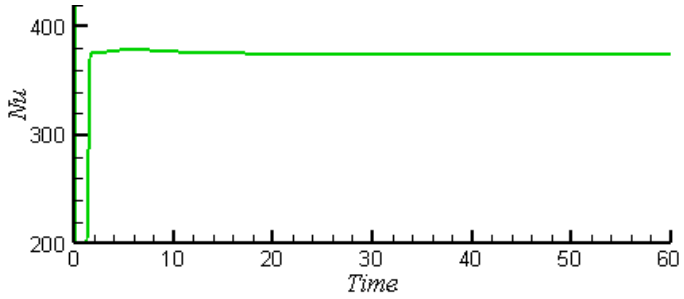

Figure 9 Transient plot of *Nu* for *Ra*=4000.

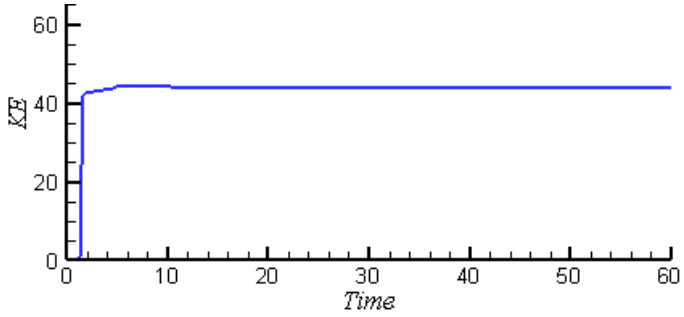

Figure 10 Transient plot of *KE* for *Ra*=4000.

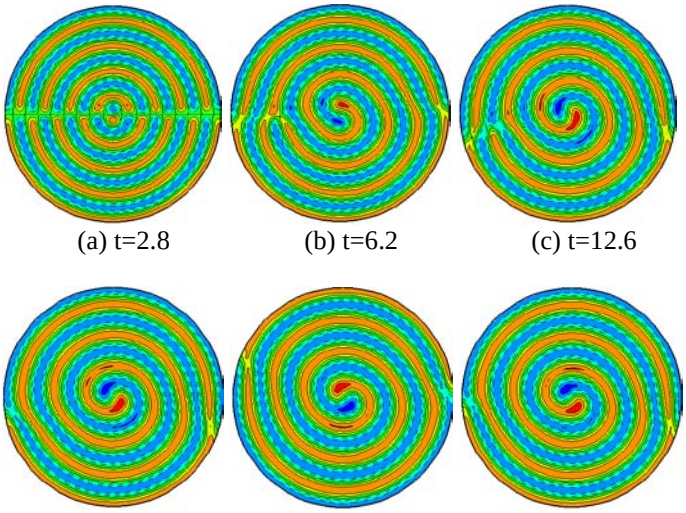

(a) t=2.8 (b) t=6.2 (c) t=12.6

(d) t=15.0 (e) t=70.6 (f) t=123.9

θ [-0.3, 0.3, (7)]

Figure 11 Isotherms at horizontal mid-height plane (z=0.5) at various times for *Ra*=4000.

Figure 12 shows transient plot of *Nu* for *Ra*=7000. Convection starts at t=0.6 and rises sharply to 476.2 and at steady rotation state *Nu*=455.5. *KE* rises sharply to a maximum of 115.3 and at steady state rotation *KE* is 110.0. Figure 14

shows the isotherms at various times. At t=0.8, the isotherms are semi-circular in shape as shown in Figure 14(a). Figure 15(a) shows that there are 19 rolls in the vertical plane perpendicular to the horizontal diameter in Figure 14 at t=0.8. Figure 14(b) shows some of the semi-circular isotherms are starting to merge together at t=2.2. At this stage the number of rolls is reduced to 17 as shown in Figure 15(b). The spiral formation starts to take shape at t=3.8 as shown in Figure 14(c) and the number of rolls is further reduced to 15. At t=7.3, Figure 14(e) shows the isotherms are now in a spiral formation. At the same time, Figure 15(e) shows 13 rolls in the vertical plane. This spiral formation starts to rotate in a counter-clockwise direction. The period of steady state rotation is 45.8.

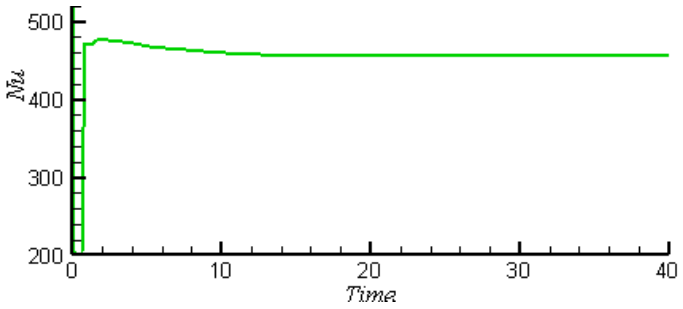

Figure 12 Transient plot of *Nu* for *Ra*=7000.

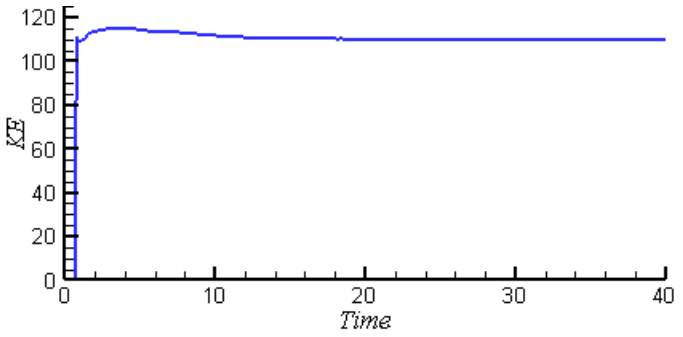

Figure 13 Transient plot of *KE* for *Ra*=7000.

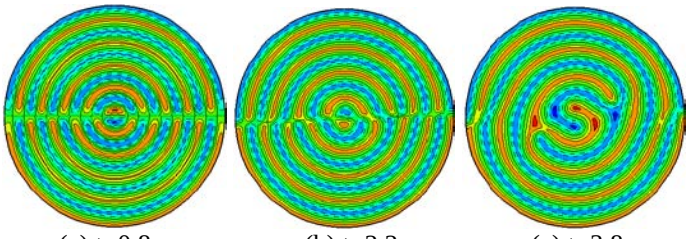

(a) t=0.8 (b) t=2.2 (c) t=3.8

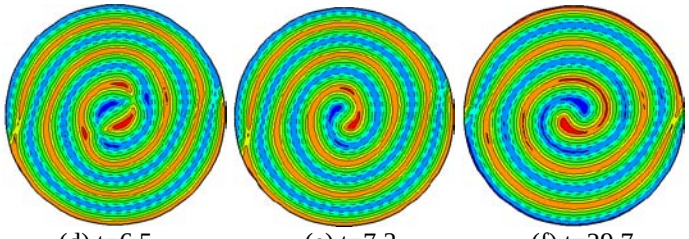

(d) t=6.5 (e) t=7.3 (f) t=29.7

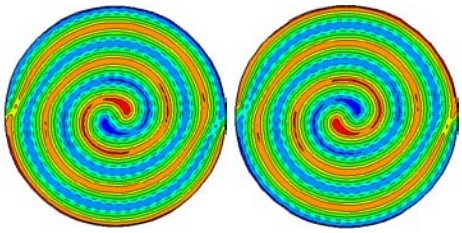

(g) t=52.2 (h) t=75.5

θ [-0.3, 0.3, (7)]

Figure 14 Isotherms at horizontal mid-height plane (z=0.5) at various times for *Ra*=7000.

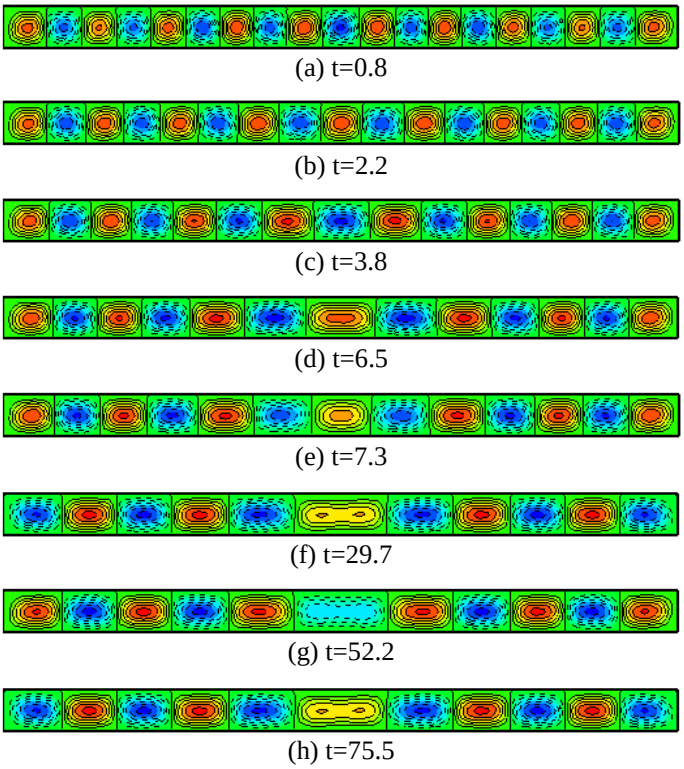

(a) t=0.8

(b) t=2.2

(c) t=3.8

(d) t=6.5

(e) t=7.3

(f) t=29.7

(g) t=52.2

(h) t=75.5

Figure 15 Contour plots of ψ_ϕ [-7.0,7.0, (13)] in the vertical plane for *Ra*=7000.

When *Ra* is increased to 10^4, convection starts at t=0.424. *Nu* rises sharply reaching a maximum value of 520. *Nu*=520.0 during the steady rotation. The maximum value of *KE* is 191.0 and during steady rotation it is 175.0. Figure 16(a) shows convection starts near the vertical wall of the cylinder and increases towards the centre. This is different from that for *Ra*=1900 shown in Figure 4(a). By t=0.6, convection is stronger near the centre while the convection near the walls become weaker. At t=0.7, all the convection is of the same strength throughout the mid-height plane. Figures 16(d), (e) and (f) show the formation of the spiral. This is different from that for *Ra*=7000 shown in Figures 14(c), (d) and (e). The spiral also unwinds before it starts to rotate in a counter clockwise direction.

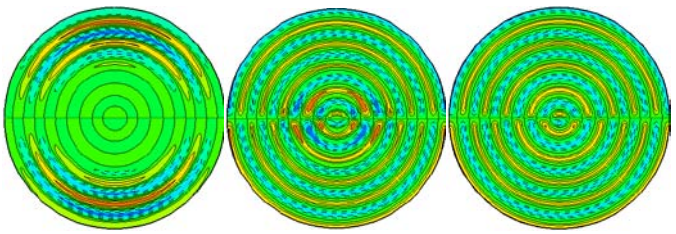

(a) t=0.5 (b) t=0.6 (c) t=0.7

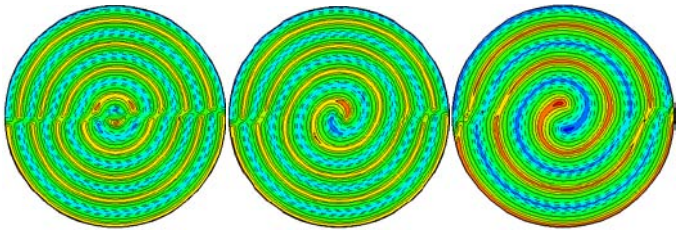

(d) t=1.7 (e) t=2.1 (f) t=7.8

θ [-0.35, 0.35, (9)]

Figure 16 Isotherms at horizontal mid-height plane (z=0.5) at various times for Ra=10^4.

Figure 17 and 18 show the transient plot of *Nu* and *KE* respectively for Ra=2x10^4. Convection starts at t=0.252 and *Nu* reached a maximum value of 659.2 at t=0.76. During the steady rotation, *Nu*=558.5. The maximum value of *KE* is 478.8 and at steady rotation it is 404. Figure 19(a) shows convection starts near the vertical wall with the formation of semi-circular arcs of isotherms. At t=0.55, these semi-circular isotherms starts to merge to form different isotherms shapes. At t=4.6, almost parallel isotherms are formed before they form a spiral by t=11.7. The spirals rotate in a clockwise direction with a period of 18.72. Figure 20(a) shows 23 rolls in the vertical plane at t=0.43. This is reduced to 19 at t=1.04and at t=2.7 there are 13 rolls. During the steady rotation, the number of rolls is between 7 and 9.

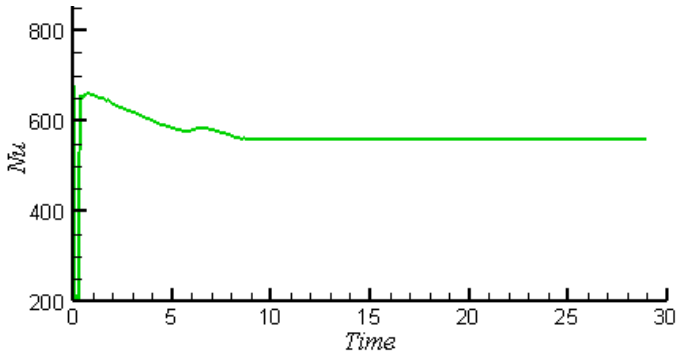

Figure 17 Transient plot of *Nu* for Ra=2x10^4.

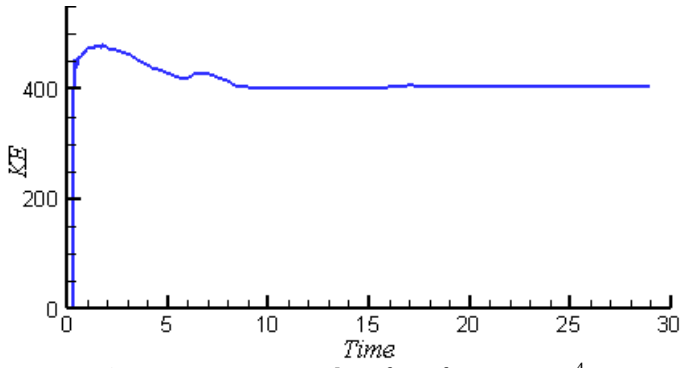

Figure 18 Transient plot of *KE* for Ra=2x10^4.

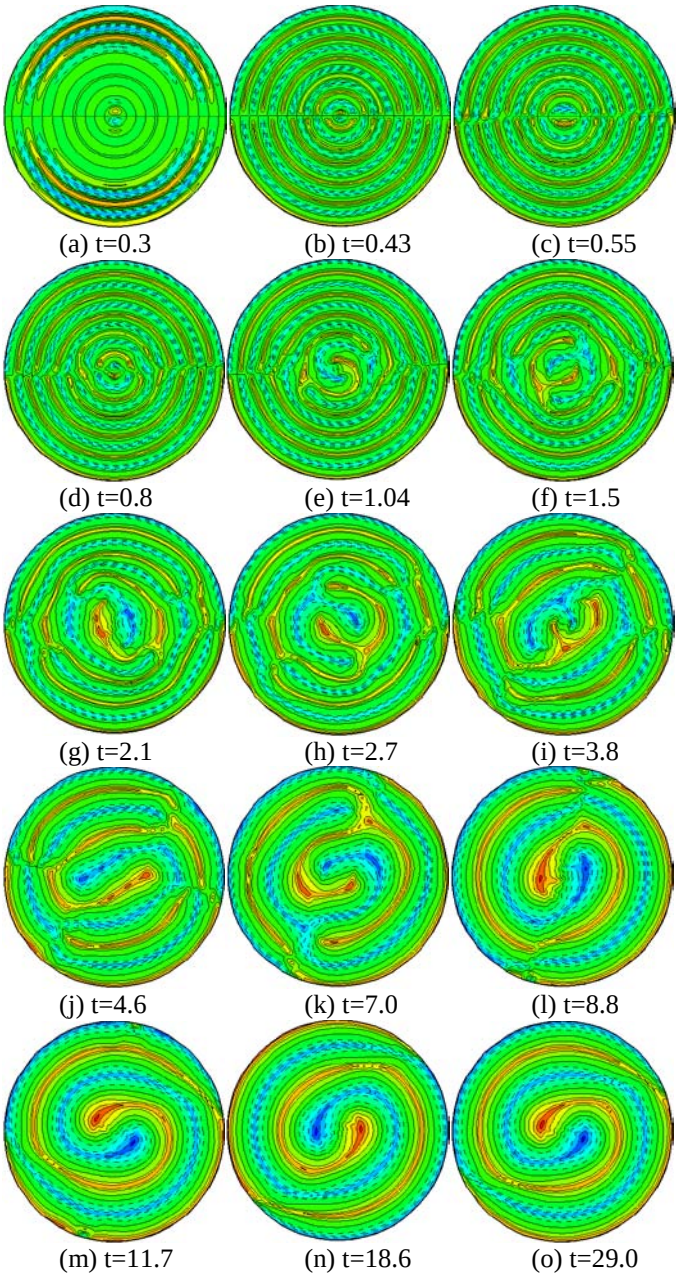

(a) t=0.3 (b) t=0.43 (c) t=0.55

(d) t=0.8 (e) t=1.04 (f) t=1.5

(g) t=2.1 (h) t=2.7 (i) t=3.8

(j) t=4.6 (k) t=7.0 (l) t=8.8

(m) t=11.7 (n) t=18.6 (o) t=29.0

θ [-0.4, 0.4, (11)]

Figure 19 Isotherms at horizontal mid-height plane (z=0.5) at various times for Ra=2x10^4.

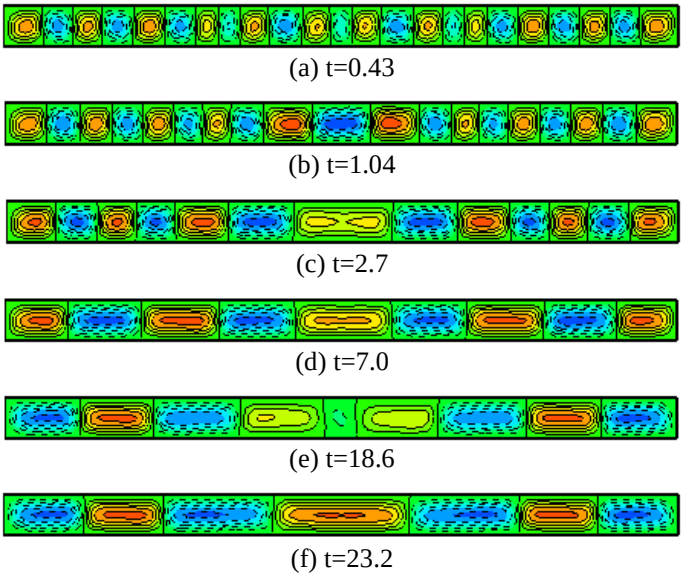

Figure 20 Contour plots of ψ_ϕ [-15.0,15.0, (13)] in the vertical plane for Ra=2x10^4.

CONCLUSION

In the range of *Ra* studied, there is always a pure conduction phase before convection starts. The duration of this pure conduction is reduced as *Ra* increases. The initial convection starts near the axis of the cylinder for low Rayleigh numbers and moves away from the axis as *Ra* increases. The initial number of rolls in the vertical plane increases as *Ra* increases. For *Ra*>2000, a spiral structure is formed which rotates about the axis of the cylinder. This spiral formation can be simple or complex changes in the structure of the isotherms. The frequency of the spiral rotation increases as *Ra* increases. The rotation can either be clockwise or counter clockwise.

REFERENCES

[1] Busse, FH and Whitehead, JA (1971), Instabilities of Convection Rolls in a High Prandtl Number Fluid, *J. Fluid Mech.*, Vol. 47, pp 305-320.

[2] Kessler, R (1987), Nonlinear Transition in Three-dimensional Convection, *J. Fluid Mech.*, Vol. 174, pp 357-379.

[3] Stella, F, Guj, G and Leonardi, E (1993), The Rayleigh-Bénard Problem in Intermediate Bounded Domains, *J. Fluid Mech.*, Vol. 254, pp 375-400.

[4] Stork, K and Müller, U (1972), Convection in boxes: experiments, *J. Fluid Mech.*, Vol. 54, pp 599-611.

[5] Davis, SH (1967), Convection in a box: linear theory, *J. Fluid Mech.*, vol. 30, pp 465-478.

[6] Müller, G, Neumann, G and Weber, W (1984), Natural Convection in Vertical Bridgman Configurations, *J. Crystal Growth*, Vol. 70, pp 78-93.

[7] Leong, SS (2002), Numerical Study of Rayleigh-Bénard Convection in a Cylinder, *Numerical Heat Transfer*, Part A - Applications, Vol. 41, No. 6-7, pp. 673-683.

[8] Liu, J and Ahlers, G (1997), Rayleigh-Bénard Convection in Binary-gas Mixtures: Thermophysical Properties and the Onset of Convection, *Phy. Review E*, Vol. 55, no.6, pp 6950-6968.

[9] Cioni, S, Ciliberto, S and Sommeria, J (1997), Strongly turbulent Rayleigh-Bénard convection in mercury: comparison with results at moderate Prandtl number, *J. Fluid Mechanics*, Vol. 335, pp 111-140.

[10] Samarskii, AA and Andreyev, VB (1963), On a high-accuracy difference scheme for an elliptic equation with several space variables, *USSR Comp. Math. and Math. Phys.*, Vol. 3, pp 1373-1382.

[11] Le Bail, RC (1972),Use of fast Fourier transform for solving differential equations in physics., *J. Comp. Phys.*, vol. 9. pp 440-465.

[12] Cooley, JW and Tukey,JW (1965), An algorithm for the machine calculation of complex Fourier series, *Maths. Comput.*, vol. 19, pp 297-301.

[13] Leong, SS (1984), *Natural Convection in Cylindrical Containers*, Ph.D. thesis, The University of New South Wales, Sydney, New South Wales.